SANDIA REPORT

SAND2001-3612
Unlimited Release
Printed November 2001

Silicon Three-dimensional Photonic Crystal and its Applications

Shawn Lin, J. G. Fleming, S. K. Lyo

Prepared by
Sandia National Laboratories
Albuquerque, New Mexico 87185 and Livermore, California 94550

Sandia is a multiprogram laboratory operated by Sandia Corporation,
a Lockheed Martin Company, for the United States Department of Energy under Contract DE-AC04-94AL85000.

Sandia National Laboratories

Issued by Sandia National Laboratories, operated for the United States Department of Energy by Sandia Corporation.

Available to DOE and DOE contractors from
U.S. Department of Energy
Office of Scientific and Technical Information
P.O. Box 62
Oak Ridge, TN 37831

Telephone: (865)576-8401
Facsimile: (865)576-5728
E-Mail: reports@adonis.osti.gov
Online ordering: http://www.doe.gov/bridge

Available to the public from
U.S. Department of Commerce
National Technical Information Service
5285 Port Royal Rd
Springfield, VA 22161

Telephone: (800)553-6847
Facsimile: (703)605-6900
E-Mail: orders@ntis.fedworld.gov
Online order: http://www.ntis.gov/ordering.htm

SAND 2001
Unlimited Release
Print 2001

Silicon Three-dimensional Photonic Crystal and its Applications

Shawn Lin
Photonic Research Department

J.G. Fleming
MEMS and Novel Si Science and Technology

S.K. Lyo
Semicoductor Materials and Device Science

Sandia National Laboratories
P.O. Box 5800
Albuquerque, NM 87185

ABSTRACT

Photonic crystals are periodically engineered “materials” which are the photonic analogues of electronic crystals. Much like electronic crystal, photonic crystal materials can have a variety of crystal symmetries, such as simple-cubic, closed-packed, Wurtzite and diamond-like crystals. These structures were first proposed in late 1980’s. However, due mainly to fabrication difficulties, working photonic crystals in the near-infrared and visible wavelengths are only just emerging. In this article, we review the construction of two- and three-dimensional photonic crystals of different symmetries at infrared and optical wavelengths using advanced semiconductor processing. We further demonstrate that this process lends itself to the creation of line defects (linear waveguides) and point defects (micro-cavities), which are the most basic building blocks for optical signal processing, filtering and routing.

INTRODUCTION

The drive for miniature photonic devices has been hindered by our inability to tightly control and manipulate light. Moreover, photonics technologies are typically not based on silicon and, until recently, only indirectly benefited from the rapid advances being made in silicon processing technology. In this report, the successful fabrication of 3D photonic crystals using silicon processing will be discussed.. This advance has been made possible through the use of integrated circuit (IC) fabrication technologies and may enable the penetration of Si processing into photonics. This class of 3D photonic crystal is particularly promising for guiding, trapping and switching of light. The accomplishments of this LDRD funded project are described below.

Chapter 1

A Three-Dimensional Photonic Crystal with Stop Band between 1.35 and 1.95 Microns

A combination of advanced silicon processing techniques was used to create three-dimensional (3D) photonic crystals with a 180 nanometer minimum feature size. The resulting 3D crystal displays a strong stop band at optical wavelengths, between λ=1.35 and 1.95μm. This is the smallest 3D crystal ever achieved with a complete 3D photonic band gap.

The ability to confine light in three dimensions (3D) would have important implications for quantum optics and quantum-optical devices: the localization of light to a fraction of a cubic wavelength, and thus the realization of single-mode light-emitting diodes, is but one example. Photonic crystals, the optical analogues of electronic crystals, provide a means of achieving these goals. Combinations of metallic and dielectric materials can be used to obtain the required 3D periodic variation in dielectric constant, but metallic dissipation will limit its application at optical wavelengths, λ. On the other hand, 3D photonic crystals, fabricated in low-loss gallium arsenide using the “drilling” method, showed only a weak stop band, that is the range of frequencies at which propagation of light is forbidden, centered at λ~1.3 μm. Here, we describe the successful realization of a silicon based 3D photonic crystal with a stop band between λ=1.35 and 1.95 μm. This is particularly important since the new 3D crystal encompasses a good deal of the spectrum of interest in optical communications and demonstrates that active structures can now be fabricated down to the band edge of silicon.

As in our previous work, we used the layer-by-layer design to fabricate our photonic crystal because of its relative ease of construction. This structure has been extensively described and modeled and consists of layers of one-dimensional rods with a stacking sequence that repeats itself every four layers. Within each layer the rods are parallel to each other and have a fixed pitch. The orientation of the rods on alternate layers is rotated 90° between layers. Between every other layer, the rods are shifted relative to each other by an amount equal to half the pitch between the rods. The resulting structure has a face-centered-tetragonal lattice symmetry of which a face-centered-cubic is a special case. In this work, the width of the rods was targeted at 0.18 μm, the height of the rods 0.22 μm, and the pitch of the rods 0.65 μm. The gap size is determined by the refractive index contrast of the two different materials that constitute the 3D structure and by the filling fraction of the higher index material. In our case the index contrast between the polysilicon and the surrounding air was ~3.6:1.

The 3D crystals were formed using advanced silicon MEMS (MicroElectroMechanical Systems) and IC (Integrated Circuit) processes. Six inches single crystalline silicon substrates were used throughout this work. Fig. 1 shows the schematic process flow. The minimum feature size was the 0.18 μm width of each of the silicon rods. This is considerably smaller than the minimum feature size of ~0.5 μm achievable using our current "I-line" stepper systems. We achieved this dimension using fillet processing. This approach relies upon the fact that when a thin film of material is deposited over a step and then subjected to anisotropic reactive ion etching, a thin sliver of material remains along the sides of the step. If the step height is several times greater than the thickness of the thin film deposited, then the width of the fillet will be identical, or at least proportional to the film thickness. Thin film thickness can be very tightly controlled and thicknesses on the order of 0.18 μm are commonly used.

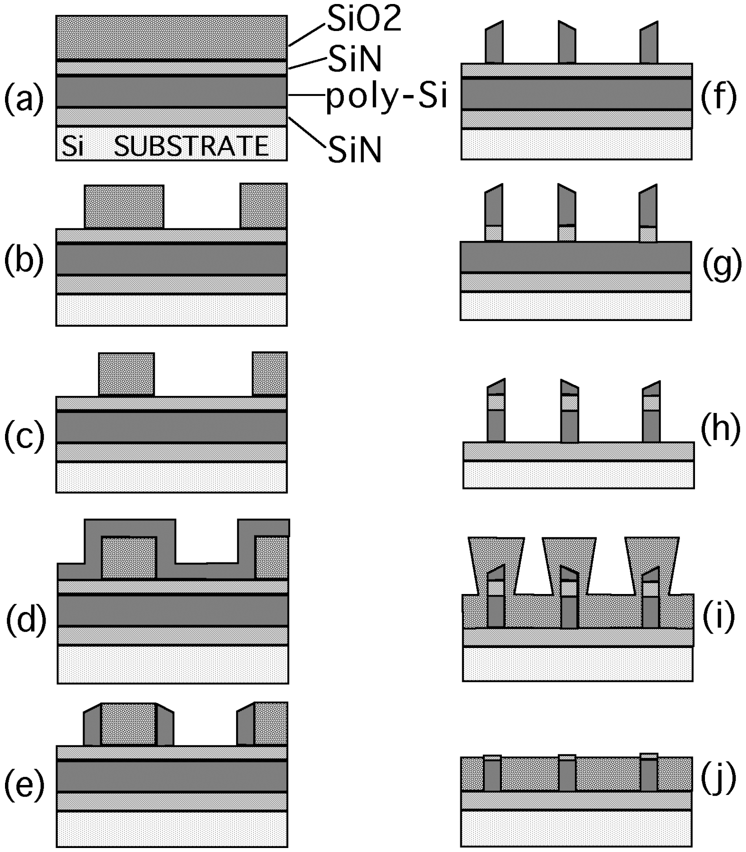

Fig.1

In the first step of the process, Fig.1(a), a thin film of polysilicon is deposited having the thickness of the desired final height of the line, 0.22 μm. The polysilicon is then capped with a thin film of silicon nitride which acts as a combination etch and CMP (Chemical Mechanical Polish) stop. The sacrificial step material is then deposited. A plasma enhanced silicon dioxide is used in this step. The layer is then photopatterned, Fig.1(b). Since the minimum dimension is attained using the fillet process, the minimum feature size is now that of the pitch of the array, 0.65 μm. After photopatterning, the oxide is anisotropically etched to just above the level of the silicon nitride layer. A 30-second wet etch in a room temperature 6:1 mixture (Ammonium fluoride: Hydrofluoric acid) is then used to isotropically remove ~90 nm of silicon dioxide, Fig.1(c). This is done to ensure that the silicon nitride is exposed and to slightly relax the minimum feature requirement of the photolithography. Polysilicon is used to form the fillet, Fig.1(d). The poly silicon is etched in a high density plasma source system, Fig.1(e). Following fillet formation, the sacrifical oxide is stripped, Fig.1(f). The fillet is then used as a mask for the etch of both the underlying silicon nitride and silicon dioxide layers, Fig.1(g)-(h). Since the height of the poly silicon fillet is greater than that of the layer being etched, the fillet itself serves as the mask.

The next critical step in the processing involves the use of CMP to maintain planarity throughout the process. The first step is to fill the gaps between the lines of polysilicon with a 0.3 µm deposition of silicon dioxide, Fig. 1(i). The wafers are then planarized back to the silicon nitride stopping layer using CMP, Fig.1(j). The CMP processing is critical since it prevents the topography generated in the first levels from being replicated in each subsequent level. At this point the entire process is repeated to form the subsequent layers of the structure. After completion of the desired number of layers, the silicon dioxide between the polysilicon lines is removed in a concentrated hydrofluoric acid/water solution with excellent selectivity between poly silicon and silicon dioxide. The parts are now ready for testing. An oblique cross-section scanning electron micrograph of a 4 level structure is shown in Fig.2. The crystal symmetry axis, <001>, is along the layer stacking direction. The rods are oriented either along <110> or <1-10>.

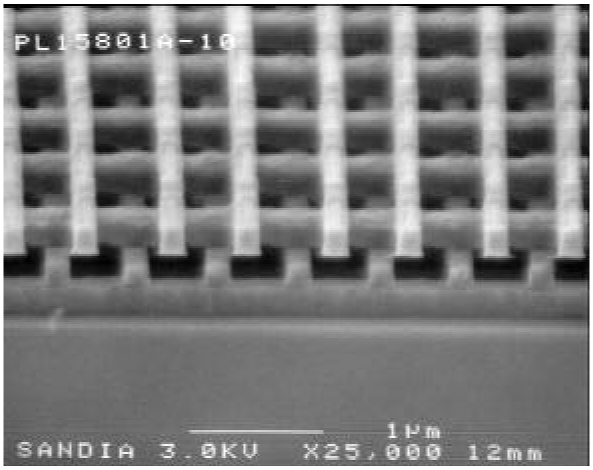

Fig.

The transmission properties of the 3D crystal was measured using a room temperature Fourier-transform infrared measurement system with a spectral range from λ=1 µm to 3 µm. Before measurement, the backside of the silicon substrate was polished to a smoothness of better than 0.2 µm to avoid significant light scattering. The sampling beam size was 2x2 mm^2, and the beam was collimated to within a 10^{o} divergence angle. The light was incident along the stacking direction, <001>, of the 3D photonic crystal and unpolarized. To find the absolute transmittance, a reference spectrum from a bare silicon wafer was first obtained along with the signal spectrum taken from a wafer with a 3D photonic crystal built on it. By ratioing the signal to the reference spectrum, the system's detector response was normalized.

The absolute transmission spectrum of light propagating along the <001> direction of the 3D photonic crystal, that is, normal to the substrate, is shown in Fig. 3. The transmittance is plotted on a logarithmic scale as a function of wavelength from 0.8 to 2.8µm. A strong transmittance dip is observed at λ=1.35 to 1.95 μm, providing convincing evidence for the existence of a photonic bandgap in the optical wavelengths. The gap extends over a spectral range of Δλ=0.6 μm; the gap to mid-gap ratio of Δλ/λ=36% is large. The development of the bandgap is also clearly evident as the number of overlayers is increased from 3 to 4. A further tilt-angle transmission measurement, similar to the one presented in reference 8,was carried out to study the angular dependent of the band gap. Light is incident along the plane spanned by <001> and <110> vectors, Fig.2, and the incident angle θ varied from 0° to 60°. The gap is systematically narrowed from Δλ=0.60 μm to Δλ=0.35 μm as θ is increased to 60°. This observed gap is close to the expected minimum gap of Δλ=0.34μm for our 3D lattice. This result is cosistent with theoretical prediction that our 3D crystal has a complete photonic band gap.

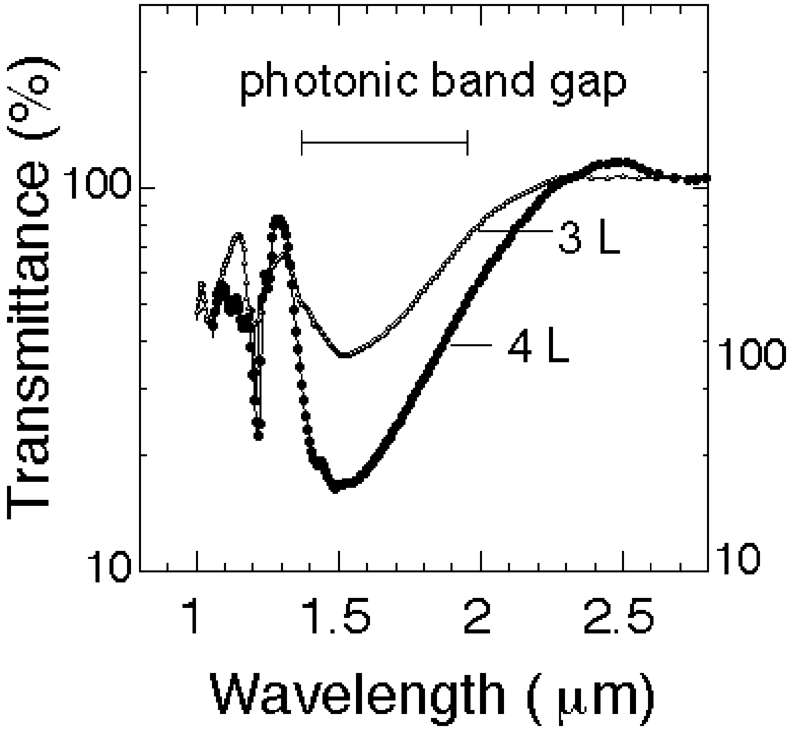

Fig.3

For comparison purposes, a transmittance plot taken from an infrared 3D crystal is also shown in the bottom panel of Fig. 3 as open circles. The design of the optical and infrared 3D crystals is identical, except their respective dimensions are different by a factor of 6.6:1. As a result, the wavelength was scaled, 6.6:1. The vertical axis is shifted downward by 10 dB for ease of comparison. Impressively, the details of the transmission spectra for both samples are almost identical, despite the ~15% layer-to-layer misalignment of the optical 3D crystal. This comparison verifies that, indeed, a photonic band gap scales linearly with device dimensions. Furthermore, it shows that the layer-by-layer design is relatively insensitive to slight process instabilities. One possible reason for this is that in this approach, defects do not tend to be cumulative. For example, during the photolithographic process the second and third layers are each aligned back to the first layer. In this way, misalignment between the first and second layers is not propagated onto the third layer. The fourth layer aligns to the second layer, however any misalignment between the second and first layers is again immaterial because of the nature of the design. This situation is very much different from that of the parts formed by the "drilling" method. In this case, small errors in any of the angles accumulate as the hole propagates into the body of the substrate.

In summary, this demonstration brings the working 3D photonic crystals into wavelength regimes where most optoelectronic devices operate, i.e. 1.3 and 1.5 μm. A whole variety of very exciting photonic devices, including low-loss waveguide sharp bends, high-Q resonant cavities, and single-mode light-emitting-diodes, can now be made from 3D photonic crystals.

Chapter Two

A Complete Three-Dimensional Photonic Band Gap in a Simple-Cubic Structure

The creation of a three-dimensional (3D) photonic crystal with simple-cubic (SC) symmetry is important for applications in the signal routing and 3D waveguiding of light. Using a simple stacking scheme and advanced silicon processing, a 3D SC structure was constructed from a 6-inch silicon wafer. The SC structure is experimentally shown to have a complete 3D photonic band gap in the infrared wavelength. The finite size effect is also observed, accounting for a larger absolute photonic band gap.

One unique application of a photonic crystal is the routing and guiding of light in all three-dimensions (3D). Today, the layer-by-layer lattice derived from the diamond lattice is perhaps the most widely studied 3D photonic crystal structure because it has a large complete photonic band gap. It may be fabricated using a combination of layer-stacking scheme and standard silicon microelectronic processes. Unfortunately, the stacking structure has a 90-degree rotational symmetry only in the stacking plane that consists of the x and y axes, but not in the x-z and y-z plane (z is the stacking direction). On the other hand, a simple-cubic (SC) lattice structure is symmetrical with respect to x, y, z rotations and, therefore, is the most natural platform for constructing photonic crystal waveguide and bends. Theoretical investigation suggests that it is possible to create such an SC structure with a complete photonic band gap. A successful demonstration of a complete band gap would require a mapping of dispersion relationship along major crystal symmetry directions. But, so far, any experimental attempt has only found a partial gap in the microwave wavelength. This paper reports observation of a complete 3D photonic band gap in an SC structure at infrared wavelengths.

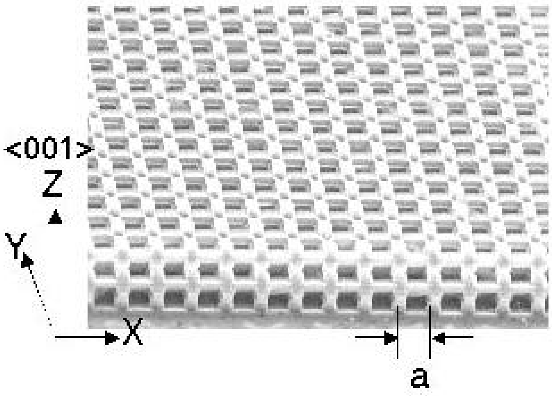

Fig.1a

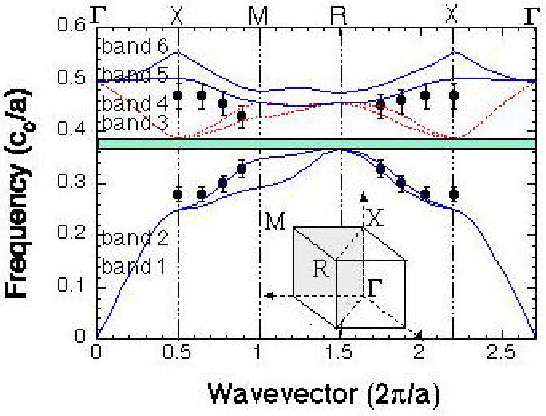

Fig.1b

The 3D SC photonic crystal was fabricated using advanced silicon processing techniques. The structure consists of layers of interconnected square rods, joined by vertical posts to form an SC lattice. A scanning-electron-microscopy image of the fabricated sample structure is shown in Fig.1 (a). The rod has a width of w=0.8 μm and the rod-to-rod spacing is a=3.2 μm. The dielectric filling fraction of the SC structure is 19%. As the first step of the fabrication process, the square frame of width w is lithographically patterned and etched. At the second step, a silicon dioxide layer is deposited to cover the patterned structure. The third step of the process is to use chemical-mechanical-polishing (CMP) to planarize the silicon dioxide surface. The fourth step is to deposite poly-silicon and then pattern it into the square posts, also with a width of 0.8μm and a height of h=2.4 μm. As the final step, silicon dioxide is deposited and then planarized using CMP. This completes the process for making a one-unit cell. The process may be continued to build more unit cells. A fraction of unit cell may also be constructed by adjusting the post height.

A computed dispersion relationship for the SC lattice is plotted in Fig.1(b). The frequency, f, and wavevector, k, are both expressed in normalized units, i.e. $f(c_o/a)$ and $k(2\pi/a)$, respectively. The dispersion is computed using two structure parameters: a silicon refraction index of n=3.6 and a filling fraction of 19%. The lowest six bands are shown. Band-1 and band-2 are the photonic valence bands (VB). Band-3 to band-6 are the photonic conduction bands (CB). A schematic of the first Brillioun zone of a SC lattice is also shown in the inset. The Γ, X, M and R are symmetry points at <000>, <001>, <011> and <111> respectively. The VB is doubly degenerate at both the X- and R-points. The CB is also doubly degenarate at X-point and triply degenerate at the R-point because of a three-fold rotational symmetry. For the lowest CB, its dispersion has a slight ~6% variation along Γ−R, and a much larger ~20% variation along Γ−X and X-M. The complete band gap is defined by the VB maximum at the R-point and the CB minimum at the X-point. The gap to mid-gap ratio is calculated to be 5% for an infinite crystal.

To test the 3D SC photonic crystal sample, tilt-angle transmission measurements were carried out using a Fourier-transform infrared measurement system. Before measurement, the backside of the silicon substrate was polished to a smoothness of better than 0.2 μm to avoid significant light scattering. To find the absolute transmittance (T), a transmission spectrum taken from a 3D crystal sample was normalized to that of a bare silicon wafer. To probe the dispersion relationship along the major symmetry axis, the sample is mounted on a two-axis rotational stage. Depending on the sample tilt direction, the dispersions from Γ-X to Γ-R and Γ-X to Γ-M can both be measured. Our experimental setup is capable of taking the spectrum over a rotational angular span from $\theta=0^o$ to 60^o, measured from the surface normal, i.e. <001> direction.

The transmission spectrum of light propagating along <001> direction of the SC lattice is shown in Fig. 2 as open triangles. The incident light is unpolarized. The photonic lattice consists of two unit-cells. The spectrum shows a pronounced dip centered around λ=8 μm, indicating the existence of photonic band gap along Γ−X direction. The gap extends over a wide range from λ_1=6.7 μm to λ_2=11.2 μm, or equivalently, f_1=0.47 c_o/a and f_2=0.28 c_o/a. The measured band edges f_1 and f_2 is to be compared to the calculated values, f_1(cal.)=0.39 c_o/a and f_2(cal.)=0.26 c_o/a. For f_1, the agreement between experiment and theory is only moderate. For f_2, the agreement is excellent. The measured Γ-X gap-to-mid-gap ratio of % is compatible with that of the layer-by-layer diamond lattice structure.

Three tilt-angle spectra were also shown in Fig.2 as solid dots. The light incident angle is systematically tilted away from Γ-X toward Γ-R. The tilt angles are $\theta = 20^o$, 40^o and 60^o respectively. For clarity purpose, the corresponding spectra are displaced vertically by 20% relative to each other. The positions of band edges move as θ is increased. More specifically, the VB edge shifts monotonically from $\lambda_2=11$ μm at $\theta=0^o$ to a shorter wavelength of $\lambda_2=9.7$ μm at $\theta= 60^o$. At the same time, the CB edge only changes slightly from $\lambda_1=6.5$ at $\theta=0^o$ to $\lambda_1 \sim 7.2$ μm at $\theta= 60^o$. Such a flat dispersion along Γ-X-R is consistent with the prediction of our band structure calculation. Despite the shifts in band edges, a large band gap still exists from λ ~ 7.2 to 9.7 μm (or f=0.33 to 0.45 c_o/a) at the largest tilt angle of $\theta=60^o$.

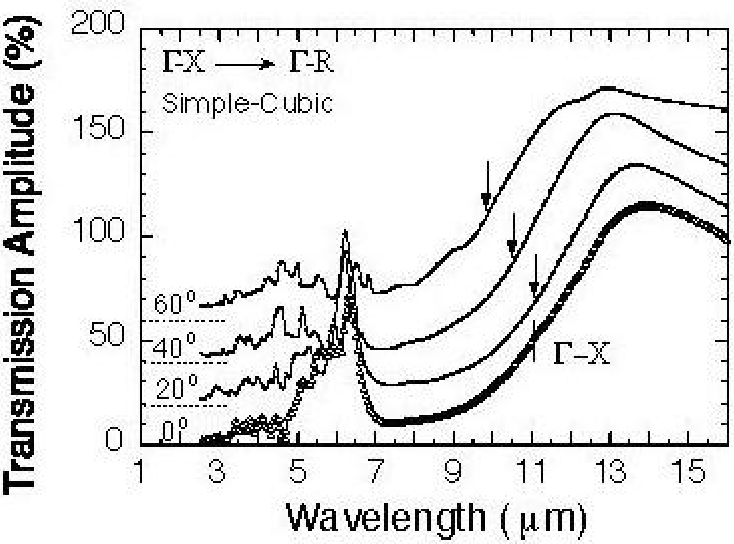

Fig.2

To probe the dispersion from Γ-X to Γ-M, a similar tilt-angle transmission measurement was also carried out. In Fig,3, the open triangular dots represent the normal incident spectrum, and the solid dots represent the tilt-angle spectra taken at $\theta=20^o$, $40^o$and 60^o, respectively. The evolution of band edges are quite similar to those observed for the case of Γ-X to Γ-R. The only exception is that the CB edge shifts stronger to long wavelength, from $\lambda_1=6.5$ to ~7.5 μm, as θ is increased to 60^o. Again, a large band gap exists from λ ~ 7.5 to 9.7 μm (or f=0.33 to 0.43 c_o/a) at the largest tilt angle of $\theta=60^o$.

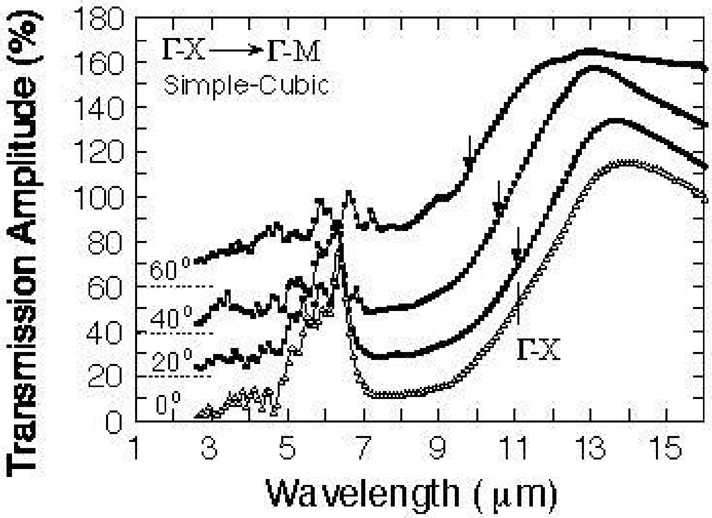

Fig.3

The measured band edges (open dots) along Γ-X-R and Γ-X-M are summarized in the calculated dispersion shown in Fig.1(b). The corresponding wavevectors are deduced from the free space incident angles θ. The maximum k values are near the zone edges M and R within 20% and 30% respectively. While theory and experiment agree well at the VB edge, the agreement at the CB edge is not as good. The measured CB edge frequency at Γ-X is about 20% higher than the computed band-3 and-4 edges. The cause of this discrepancy will be discussed in the following paragraph. Nonetheless, from the movement of band edges near the M- and R-points, the absolute gap size is expected to be smaller but close to the measured minimum band gap at the M-point of $\Delta\lambda = (9.7 - 7.5) = 2.2\mu m$.

The discrepancy between theory and experiment at the CB edge may be attributed to three factors: the finite size effect, lattice structure disorder, and wavefunction symmetry consideration. Even though our 3D crystal extends almost infinitely in the stacking plane (i.e. > 1,000 unit cells), it has a finite thickness along the stacking direction (only two-unit cells). This finite size disrupts the wavefunction of Bloch states in the crystal and changes its energy-dispersion. When lattice has structural disorder or imperfections, crystal periodicity is disrupted and energy dispersion modified. Such a disruption has been found to affect the higher energy CB-states more than the VB-states. This finding is consistent with our experimental observation.

To quantify this hypothesis, a further transfer matrix calculation is needed that calculates the transmittance of light incident on a finite thickness slab of a photonic crystal sample. Such a calculation is useful in the interpretation of experimental transmission data. In Fig.4, the calculated transmission spectra are shown for three different sample thickneses, i.e. 2, 6 and 12 unit cells, respectively. The light is incident along the stacking direction. The calculated attenuation is ~4dB/ cell. For the two unit cell sample, the CB and VB edges are at λ_1=6.8 and λ_2=12.6 μm (or f_1= 0.47 and f_2= 0.25 c_o/a), respectively. The agreement of results from our transfer matrix method and our measurement are excellent. As the sample thickness is increased to 6 and 12 unit cells, the band edge positions change. The VB edge becomes sharper, more well-defined, and moves from λ_2=12.6 to 11.7 µm. The CB edge maintains its sharpness, shifts systematically from λ_1= 6.8 to 7.4 µm (or from f_1= 0.47 down to 0.43 c_o/a), and starts approaching the band structure computed value of f_1= 0.39 c_o/a within ~10%. The effect of disorder, originating from the non straightness of the post sidewall, may also contribute to the discrapency. Detailed analysis of it will be presented elsewhere.

It is well-documented that the symmetry consideration may prevent coupling of light into certain bands in the energy-dispersion. For example, incoming plane waves with an even symmetry cannot be coupled into odd-symmetry Bloch states in the photonic crystal. However, for our 3D crystal, the wavefunction of band-3 and -4 at Γ-X are symmetrical with respect to the incoming wavevector of light. It is unlikely that coupling to band-3 and -4 is forbidden, and the observed CB originates from Band-5.

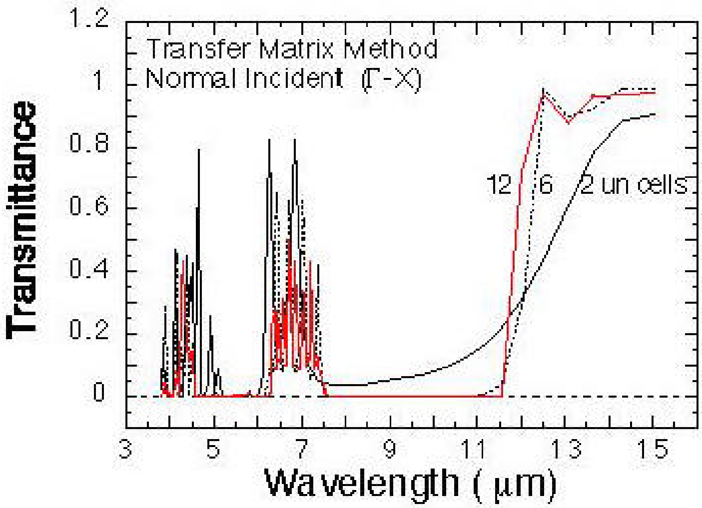

Fig.4

In summary, the observation of a complete photonic band gap in a SC lattice structure is reported in the infrared wavelengths. Because of its structural simplicity, a 3D SC photonic crystal promises efficient waveguiding and routing of light in all three dimensions. The observed absolute gap is larger than the computed value and is attributed to the finite size of photonic crystal along the stacking direction.

Chapter Three

Enhancement and Suppression of Thermal Emission by a Three-Dimensional Photonic Crystal

The emission and detection of electromagnetic radiation are essential optical processes that govern performance of lasers, detectors and solar cells. Through light-photonic crystal interaction, a three-dimensional (3D) photonic crystal offers a novel way to alter such optical processes. Experimental realization is done by building a thin slab of 3D photonic crystal onto a silicon material. The 3D crystal structure is found to be highly effective in suppressing silicon thermal radiation in the photonic band gap spectral regime. Emission is also enhanced in the photonic passbands. At passband resonant frequencies, a thin slab of 3D photonic crystal actually acts like a planar blackbody.

A three-dimensional (3D) photonic crystals is an artificially engineered, periodic dielectric material that exhibits bands and gaps in its photonic density-of-states (DOS) spectrum. Inside a photonic band gap, photonic DOS vanishes, and no electromagnetic (EM) waves are allowed to propagate. Within the photonic pass bands, oscillations in DOS occur, corresponding to transmission resonances inside the photonic crystal.

One unique application of the 3D photonic band gap is the modification of spontaneous emission. The band gap is used to establish a strongly confined optical environment, called cavity, for light trapping and size quantization. The quantization alters photonic DOS inside the cavity, leading to the modification of spontaneous emission of atoms or semiconducting materials. The same photonic band gap effect may also be used to suppress thermal emission, as it is an EM radiation. However, despite of its intricate DOS spectrum, consequences of 3D photonic passband are largely unknown, either theoretically or experimentally. Its potential influence on the emission or absorption process of a material is also unexplored.

In the work reported here, a silicon 3D photonic crystal is created and its effect on silicon thermal emission studied. The 3D crystal is found to be highly effective in suppressing silicon thermal radiation in the photonic band gap spectral regime. Surprisingly, in the photonic passbands, thermal emission intensity is enhanced. At transmission resonance frequencies, it even reaches the blackbody limit. The ability of 3D photonic crystals to alter surface emittance and absorptance may enhance performance of lasers, detectors, solar cells and infrared thermal image control.

The 3D photonic crystal has a diamond crystal symmetry and was fabricated using an advanced silicon processing. Details of the fabrication process have been reported previously. Briefly, the crystal consists of layers of one-dimensional silicon rods with a stacking sequence that repeats itself every four layers, repeating distance c. Within each layer, the axes of the rods are parallel to each other with a pitch of d=4.2 μm.

The orientation of the axes is rotated by 90^o between adjacent layers. Between every other layer, the rods are shifted relative to each other by 0.5 d [11]. The resulting structure has a face-center-tetragonal lattice symmetry. For the special case of c/d = 1.414, the lattice can be derived from a face-centered-cubic unit cell with a basis of two rods, i.e. the diamond lattice. The width of the rod is W =1.2 μm, and the filling fraction of the high dielectric silicon material is 28%. At this filling fraction, the 3D crystal has a large photonic band gap covering the infrared wavelength range from λ = 9-15 μm.

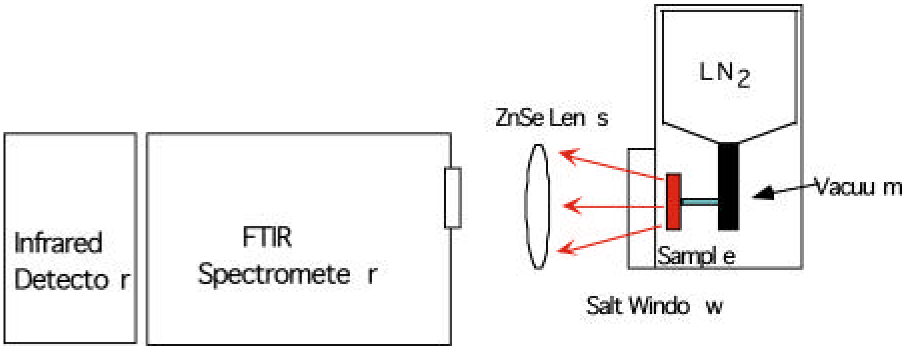

Fig.1a

To measure infrared thermal emission, the experimental setup must be properly configured such that background thermal emission is eliminated and, at the same time, sample emission intensity enhanced. To achieve this goal, the sample was placed in a liquid-nitrogen cooled (T=77K) vacuum chamber and heated to T ~ 410 K. In Fig.1(a), a schematic of such a measurement setup is shown. At low temperatures, T = 77 K, the unwanted thermal emission from the sample holder is minimized. In vacuum conditions, no air is heated and contributes to background thermal emission. Heating is also necessary to increase the thermal emission intensity. To insulate the heated sample from the liquid-nitrogen cold bath, the sample was mounted to a 2-inch-long ceramic post. The thermal radiation first passes through a salt-window, is collected by a ZnSe lens, and finally is fed into a Fourier-Transform-Infrared-Spectrometer for spectral analysis. A DTGS infrared photodetector was used for infrared signal detection. The salt window is transparent up to λ ~ 12 μm, is 50% transparent at λ ~ 17 μm and has a long wavelength cut-off at λ ~ 21 μm. The photodetector has a fairly flat spectral response in the infrared.

The detail of the sample arrangement and experimental configuration is shown in Fig.1 (b). The sample consists of two pieces of identical 3D silicon photonic crystal bound back-to-back, having the silicon layer sandwiched on both sides by a thin slab of 3D crystal. The spacing between the two layers of photonic crystal is about 1.2 mm. The boundary defined by silicon and the 3D photonic crystal slab is planar. This is in contrast to a micro-cavity structure, in which the boundary is a closed contour, commonly used to study light-photonic crystal interaction.

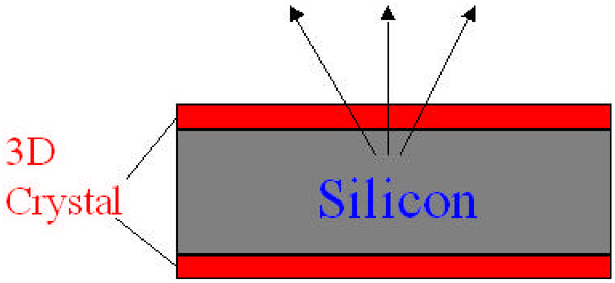

Fig.1b

In Fig. 2 (a), the emission spectrum taken from a 3-layer photonic crystal sample and a bare silicon sample are shown as red solid dots and a line, respectively. At both the long (> 18 μm) and short (< 4 μm) wavelength limits, the two curves agree well with each other. On the other hand, at the mid-wavelength range (λ = 10 to 16 μm), emission from the crystal sample is clearly suppressed. The strongest suppression is at λ ~12 μm and is indicated by the down-arrow. The suppression of thermal emission becomes stronger as the number of 3D crystal layer is increased from n = 3, 4 to 5 (see Fig. 2 (b) and (c)). The suppression is indicative of the absence of photonic DOS in the band gap regime that forbids the emission of infrared radiation in all 4 π angles.

Surprisingly, the emission intensity at λ ~ 5 to 9 μm range for the three-layer crystal sample exceeds that of silicon emission by about 30%. The enhancement is also clearly evident for the four- and five-layer samples. For the 5-layer sample, the contrast between emission suppression and enhancement is quite dramatic. Specifically, following the strong suppression in the gap regime, the emission intensity quickly rises on both sides of the band gap, intercepts the bare-si reference curve at λ = 10 and 17μm, and finally exceeds silicon emission. Pronounced oscillations also appeared in the spectrum, but only at the shorter λ =5 to 9 μm wavelength side. Also, the oscillation pattern reveals more detailed features as the number of layer is increased. The observed oscillations and their dependence on number of crystal layers suggests a correlation to the oscillating photonic DOS in a 3D photonic crystal.

For comparison purposes, a blackbody radiation curve calculated for a temperature of 410 K is also shown in Fig.2(a) as a dashed line. The silicon emission curve and blackbody curve agree with each other well, except for the gradual deviation at m. This agreement is consistent with the fact that silicon is a graybody and independently confirms the measured temperature. The line shape of a graybody is identical to that of a blackbody, but its emission intensity is weaker. The deviation is not intrinsic to the silicon emission and is caused by the long wavelength cutoff of the optical window material, as mentioned earlier.

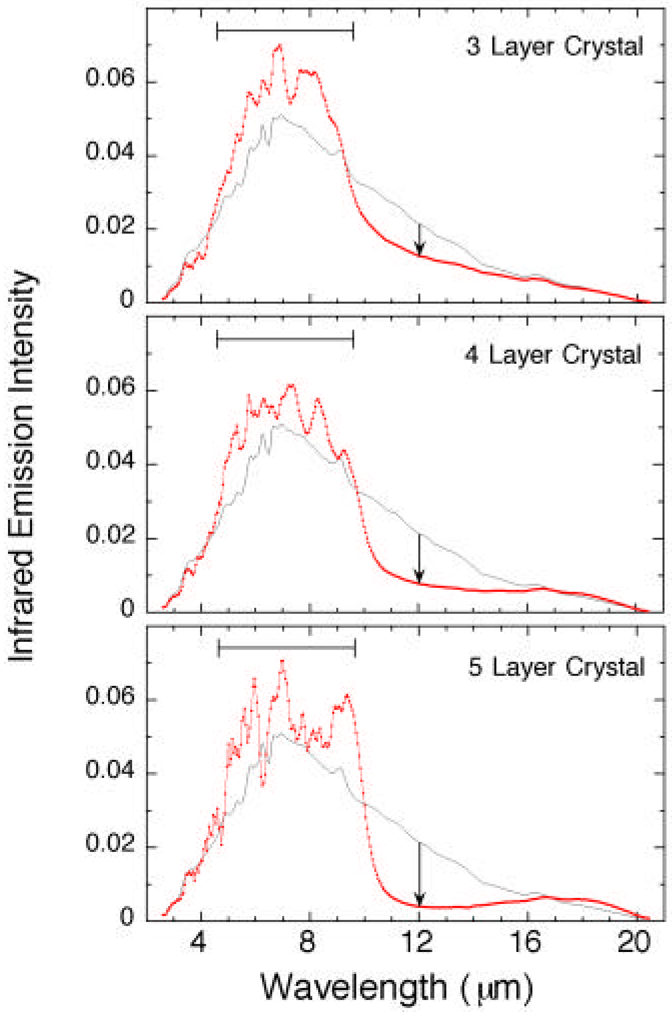

Fig.2

To obtain the absolute suppression and enhancement efficiency of a 3D photonic crystal, the two measured spectra, $f_o(\lambda)$ and $f(\lambda)$, must be normalized. The spectrum $f_o(\lambda)$ serves as a reference and is directly related to the intrinsic silicon emissivity, $E_o(\lambda)$, by: . Here, $W(\lambda)$ represents propagation loss, such as water absorption, as thermal emission passes through the spectrometer and reaches the photodetector. $D(\lambda)$ represents the combined optical window and photodetector responses. Similarly, the spectrum, $f(\lambda)$, is related to the modified emissivity, $E(\lambda)$, by: . By dividing $f(\lambda)$ into $f_o(\lambda)$, the window/detector response and water absorption loss are normalized, and a normalized emission efficiency, $E(\lambda)/E_o(\lambda)$, is obtained. Because of water absorption and background thermal radiation, the normalized emission efficiency has an experimental error of about %. One exception occurs at long wavelengths, $\lambda > 20$ μm. In this range, emission intensity is weak, and the uncertainty is estimated to be ~15%.

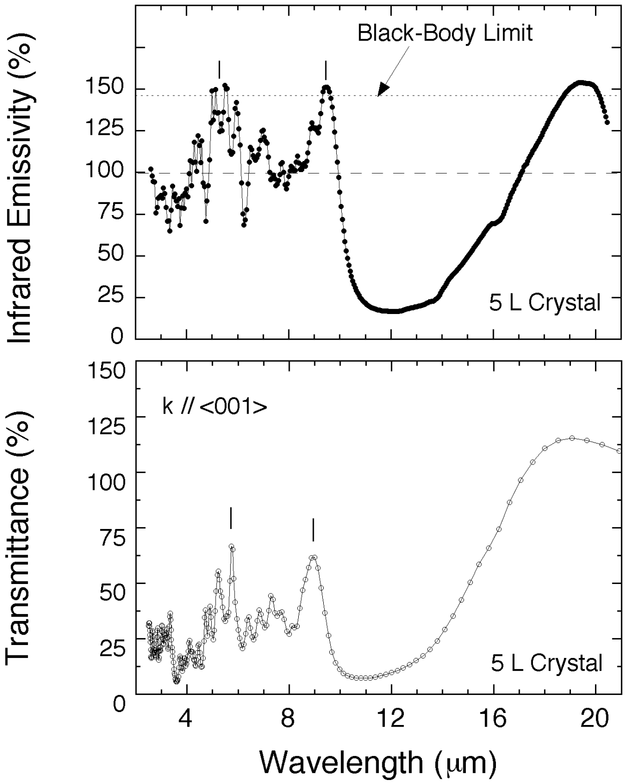

Fig.3

In Fig. 3(a), the normalized emission efficiency is plotted as a function of wavelength for the five-layer crystal sample. A clear and strong dip is observed at λ ~12 μm along with a broad bandwidth of Δλ ~ 6 μm. The dip minimum of ~15% is slightly higher than that observed, ~8%, in a straight transmission measurement with light propagating along <001> direction (Fig.3(b)). In the gap regime, thermal spectrum measures tunneling emission over all angles, which is slightly higher than that measured solely along <001>, and causes the difference. Indeed, thermal emission is three-dimensional in nature and the measured gap is truly a 3D photonic band gap. This is, to the best of our knowledge, the first direct measurement of a complete 3D photonic band gap in any 3D structure at any wavelength.

In the inset of Fig.3(a), the suppression efficiency vs. the number of layers of photonic crystal is shown as a semilog plot at λ = 12, 14, 15 and 16 μm, respectively. The straight lines show that the suppression depends exponentially on n and is consistent with the tunneling nature of light in the band gap regime. The straight line also predicts that a suppression of 99% (or equivelently a 1% emissivity) may be achieved at λ = 12 μm using an eight-layer photonic crystal. This value is to be compared to an emissivity value of 0.50 for commonly used aluminum paint and 0.15 for copper. Even for the silvered mirror, one of the lowest emissivity materials, emissivity is 0.02. Although some metallic surfaces have relatively low emissivity at room temperature, their emissivity values increase with temperature because of surface oxidation. The emissivity of oxidized aluminum and copper is high, 0.6 and 0.42, respectively. In comparison, a 3D silicon photonic crystal is more robust against such a performance deterioration for temperatures up to 800 to 900 C and is ideal for achieving an ultralow and controllable thermal emission.

Another interesting feature of the data is the unusually high emission at the passband wavelengths, λ ~ 5-10 μm and λ ~ 17-20 μm. This value not only exceeds the 30 to 70% straight transmission amplitude (Fig.3(b)), but also exceeds the silicon emission value, 100%. At oscillation maxima, the emission reaches the blackbody limit (the dashed line) within % [17]. In other words, the 3D crystal/Si structure actually acts like a planar black-body at the oscillation peaks. According to a thermodynamics law (the Kirchhoff's law [16]), a perfect emission implies a perfect absorption through the surface. This 3D crystal/Si may then be thought of as a composite material with total transparency. This property may find important solar-cell applications because it is capable of enhancing solar energy absorption efficiency by a large 30 to 40%.

One possible cause for the observed emission enhancement is photonic transmission resonances. Light inside a photonic crystal experiences multiple scattering and establishes resonances, at which total transmission is possible, and the material becomes transparent. In a photonic crystal, transmission resonances manifest themselves as maxima (or peaks) in the photonic DOS spectrum. In Fig.3 (b), the peaks and dips in passband transmittance are caused by such resonances in the photonic DOS. Comparing the emittance and transmittance spectra, shown in Fig.3(a) and (b), a clear resemblance of passband oscillations is observed. In particular, the peaks at λ ~ 5.2 and 9.4 μm in the emittance data correlate with the transmission peaks at λ ~ 5.5 and 9.0 μm. The thermal emission is 3D in nature and measured an average DOS over a range of angle (θ~40^{o}) defined by the collecting lens. This weighted averaging causes the slight shift from λ ~ 9.0 to 9.4 μm. The respective peak positions at λ ~ 20 μm also agree well with each other. This close correlation suggests that the emission enhancement is indeed a DOS effect. Theoretical calculations on 1D photonic crystal structures reached similar conclusion [18]. Yet, no calculation or experimental confirmation of it has been done up to now. This work represents the first discovery of emission enhancement brought about by a 3D photonic crystal effect.

Because of its ability to not only suppress but also enhance emission, a 3D photonic crystal may not be regarded as a purely passive filter. Perhaps, it is more appropriate to view the 3D crystal/si structure as a composite material with a new surface emissivity. It is also worth noting that a photonic crystal itself also emits thermal radiation. A five-layer crystal has a thickness of only 8 μm and a thermal mass (because of the 28% filling fraction) that is equivalent to a thin silicon layer ~2.5 μm thick. However, emission from such a small thermal mass is too weak to be measured using our current experimental setup.

Finally, to demonstrate an imaging application, two new pieces of photonic crystal sample are fabricated: one has four-layers and the other six-layers. The samples are mounted to a six-inch silicon wafer for ease of handling. Within each sample, three regions, A, B and C, corresponds to crystal structures with a band gap (A), a weaker gap (B), and no gap (C) at λ ~ 9 μm. In Fig.4 (a), an infrared thermal image of the photonic crystal sample is shown. The infrared camera has a spectral response centered at λ = 9 μm, a bandwidth of . For both samples, a darker contrast in region A is observed, signifying the blocking of thermal emission from silicon at λ = 8.7 to 9.3 μm spectral range. For the six-layer sample, a weaker but clear dark contrast also appears, consistent with a weaker gap associated with region B. In Fig.4(b), an expanded, color-coded image of the two samples is also shown. The yellow color represents the strongest infrared signal and the dark blue the weakest. An absolute quantitative comparison of the spectrum is not possible currently because detailed calibrations of thermal intensity are required. Nonetheless, this image clearly demonstrates the usefulness of a 3D photonic crystal as a means for thermal image control at the infrared wavelengths.

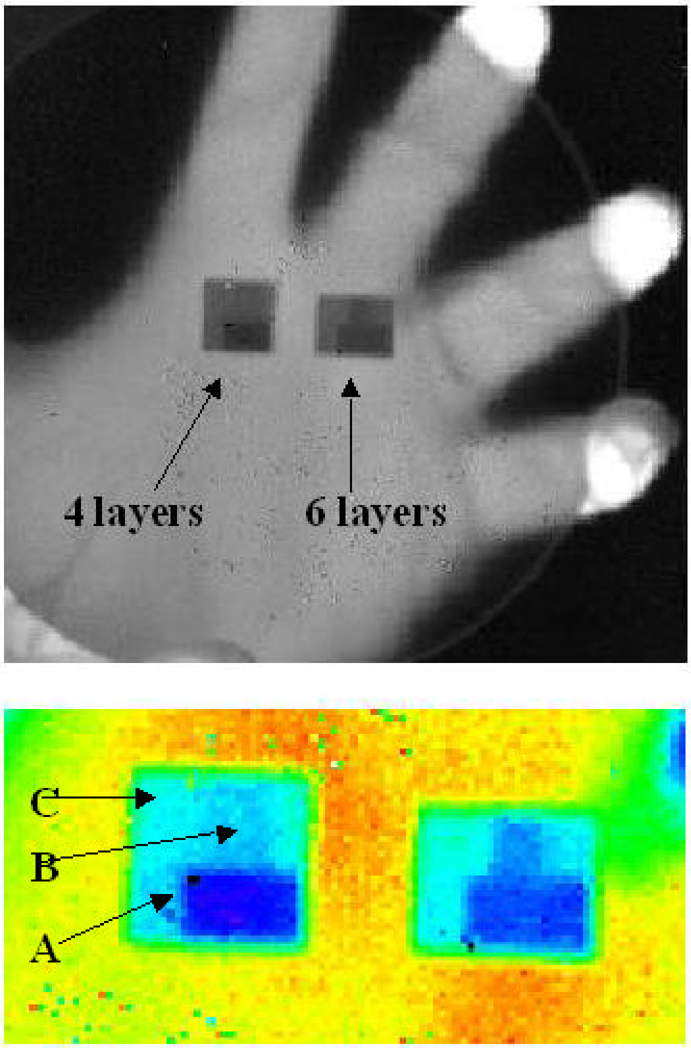

Fig.4

In summary, the first observation of thermal emissivity modification from silicon is reported using a 3D photonic crystal. The 3D crystal is found to be highly effective in suppressing the thermal emission. The surprising discovery of emission enhancement leads us to conclude that a thin slab of 3D crystal actually acts like a black-body at transmission resonances. Furthermore, through photonic DOS engineering, a 3D photonic crystal offers a fundamentally new way for altering surface emissivity and absorption. As all forms of light emission and absorption must pass through a surface, photonic crystal DOS engineering will impact the whole spectrum of light emitters and detectors ranging from infrared to visible.

Chapter Four

Photonic Band Gap Micro-Cavities in Three-Dimension

Localization of light to less than a cubic wavelength, l^3, has important quantum consequences. The creation of single mode cavities and the modification of spontaneous emission are two important examples. A defect formed inside a 3D photonic crystal provides sucn an optical environment for localizing light. Single mode defect cavities were built, for the first time, from an infrared 3D photonic crystal. A cavity state with modal volume of less than one l^3 was observed.

A photonic crystal is the optical analogue of an electronic crystal. It is a periodic dielectric structure with its dielectric constant spatially varied according to certain crystal symmetries. Much like electrons in a crystal, photonic states inside a photonic crystal are classified into bands and gaps, frequency ranges over which photons are allowed or forbidden to propagate respectively. The bands and gaps provide a fundamentally new mechanism for localizing light to less than a cubic wavelength, λ^3, which is not attainable using conventional optics.

A defect cavity may be created to trap light at a point within a 3D crystal. A defect is formed by changing the dielectric constant in a local region of the crystal. In particular, there are two classes of defects, namely the “vacancy defect” created by removing a section of the rod and an “interstitual defect” formed by adding extra dielectric materials into the crystal. The defect state may appears in the forbidden photonic band gap spectral regime, leading a strongly localized state. The strength of photonic localization is determined by the size of the band gap, which acts as a highly reflecting mirror. To maximize the band gap, dielectric contrast (or equivelently refractive index) of the two materials that constitute the 3D structure and filling fraction of the higher dielectric material must be carefully chosen.

A "layer-by-layer" stacking design was used to construct the 3D photonic crystal. The design has been extensively studied theoretically and experimentally. It consists of layers of one-dimensional rods with a stacking sequence that repeats itself every four layers. Within each layer the rods are parallel to each other and have a fixed pitch (d). The rod also has a fixed width (w) and height (h). The orientation of the rods on alternate layers is rotated 90° between layers. Between every other layer, the rods are shifted relative to each other by an amount equal to half the pitch between the rods. For the special case of 4h/d=1.414, the lattice can be derived from a faced-centered-cubic unit cell with a basis of two rods. The structure can also be derived by replacing the <110> chain of atoms in the diamond structure with the rods. For our 3D crystal, the maximum gap is achieved by having a index contrast of 3.6:1 and filling fraction of 28%. The defect state may also be tuned across the band gap by varying the defect size. In our case, vacancy defects are studied and their corresponding defect frequencies tuned by varying the removed section, with length L’, of the 1D rod.

To build the 3D crystal and defcet cavities, a combination of advanced silicon processing techniques were used. In the first step of the process, a thin film of polysilicon is deposited, photopatterned and etched. The next step in the processing involves the use of chemical-mechanical-polishing (CMP) to planarize the patterned structure. A layer of silicon dioxide (SiO_2) was deposited in between the lines of polysilicon. The wafers are then polished and planarized using CMP. The planarization step is critical since it prevents the topography generated in the first level from being replicated in the subsequent level. At this point the entire process is repeated to form a three layer structure. The fourth layer is the defect layer, where a series of vacancy defect is created having L'= 2, 15, 30 and 50μm. One top of the defect layer, three more layers were build to complete a seven layer 3D structure. After completion of the seventh layer, SiO_2 is removed by selective wet etching.

In Fig.1 (a), a cross section scanning electron microscopy (SEM) image of the defect cavity is shown. The sample is cleaved right across the middle of the defect cavity for imaging purpose.The small missing section at the fourth layer is the defect cavity. A top view SEM image of the defect cavity at the fourth layer was shown in Fig.1(b). The defect is the small vacancy of length L' along the 1D rod. The defect dimension is given by ΔV=L' x 2d x 4h, where L'=2μm, d=4.3μm and h=1.6μm. Given the mid-gap wavelength of λ~11μm, ΔV is as small as ~ $0.08\lambda^3$. For L'=15, 30 and 50μm, the corresponding ΔV is also compact: ~ 0.6, 1.2 and 2.0 λ^3. To maximize the transmission signal, defects are arranged in an array fashion. The defects are spaced by two rods along y-direction, a spacing distance of 3d=12.9μm, and seperated by a distance of L along x-direction.

To probe the localized states, both transmission and reflection measurements were carried out using a Fourier-transform infrared measurement system. Before measurement, the backside of the silicon substrate was polished to a smoothness of better than 0.2 μm to avoid significant light scattering. To find the absolute transmittance (T), a transmission spectrum taken from a 3D crystal sample was normalized to that from a bare silicon wafer. To find the absolute reflectance (R), a reflection spectrum taken from the same 3D crystal is normalized to that of a silver mirror. Our reflectance set-up is capable of taking spectrum over an angular span of $\theta=15^o$-70^o measured from the surface normal, i.e. <001> direction, and has an accuracy of %.

The absolute transmittance of light propagating through a 3D micro-cavity is shown in Fig. 2(a). The vacancy defect has a L'=2μm and ΔV~0.08 λ^3. The infrared light is incident along the stacking direction, <001>, of the 3D crystal and is un-polarized.The transmitted signal is collected by a photodetector with its receiving surface oriented along <001> direction. A schematic drawing of the measurement set-up and the defect cavity is shown in the inset. The transmittance shows a single tranasmission peak, centered at λcavity=11.2μm, indicating the existance of a cavity mode in the forbidden band gap regime. The measured transmitted signal is the evanescent leakage of strongly localized fields inside the cavity. The peak transmission amplitude is 6% and full-width-half-maximun 0.8μm, or a cavity-Q of 14. Our observation agrees well with a theoretical calculation based on a transfer matrix method. In particular, the observed peak wavelength agrees with the theoretical value (indicated as an arrow); the measured cavity-Q is also close to the predicted value of Q=13; and peak transmission amplitude of 6% is consistent with the computed one. This agreement provides independent confirmation that the observed transmission peak originates from a single mode resonant state.

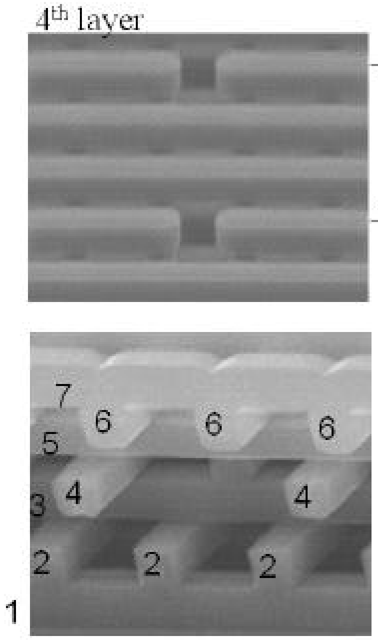

Fig.1(a) and (b)

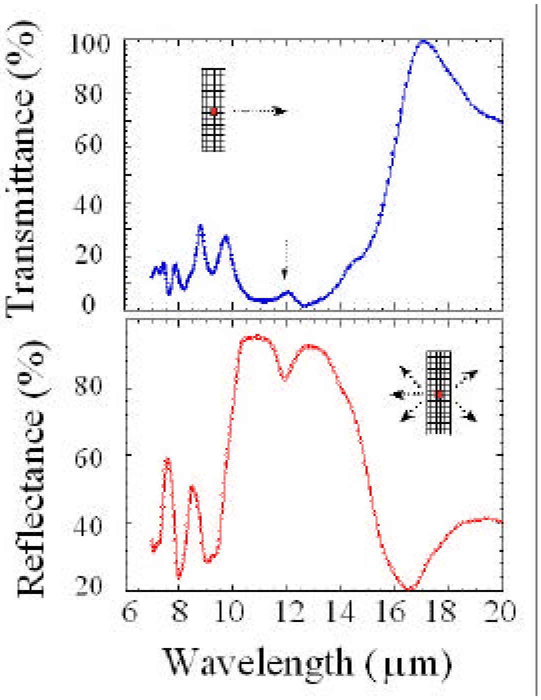

Fig.2(a) and (b)

To verify the defect cavity mode, a complimentary reflectance measurement is also carried out . The reflectance spectra was taken from the same sample at a slight tilt angle, $\theta=15^{o}$, and the measured data shown in Fig.2(b). As expected, the reflectance dip occured at the same λcavity= 11.2μm.. However, a dip amplitude of ~12% is observed which is about two times larger than the transmittance signal collected along <001>. Our observation suggests that some portion of light may be scattered away from <001> which was not detected by the <001> oriented photodetector. And yet, in a reflectance measurement, all transmitted signals, scattered or not, contribute to dip in the reflectance spectra. A schematic for the scattering picture is shown in the inset of Fig.2(a). To confirm this hyposesis, a computer simulation that collecte signals from all angle is carried out. First of all, the simulated result shows that surface scattering is not important and the source of scattering is the cavity. And secondly, it shows that indeed the integrated transmitted signal is two times larger than the <001> forward transmitted signal.

Reflectance measuremnts can also be used to verify the 3D nature of a defect cavity. If a cavity is truely three-dimensional, its modal frequency should be angular independent. This is due to the fact that such a cavity mode is established by the coherent resonance of light from all angles inside the cavity. A series of reflectance measurement was carried out over an angle $\theta=15^{o}$ - 70^{o} to investigate such an angular dependence. Our results shows that cavity frequency is angular independent for all angle tested and the defect cavity built from our 3D photonic crystal exhibits a 3D character.

To probe the wavefunction extent, localization length ε, of the localized state, defects are arranged in an array fashion. When L, distance between adajecent defects, is compatible to defect wavefunction extent in the layer plane, near-by defect cavities interact and defect modal frequency shifts. From the onset of this frequency shifting, in-plane wavefunction extent may be estimated. This gives a measure of the modal volume, ΔV_{mode}, associated with the defect cavity. Transmittance spectra taken from defects arranged with defect spacing L=10, 15 and 20μm are shown in Fig.3. The defect frequency remains essentially the same at L=15 and 20μm and shifts significantly to a longer wavelength for at L=10mm. A similar trend was also observed for a slightly larger cavity with L'=15μm. From the onset of the frequency shift, the in-plane wavefunction extent is estimated to be $\varepsilon_{//}$ ~ 10μm. The wavefunction extent along the stacking direction can also be obtained by performing transmittance measurement for samples with different number of layers. By plotting the transmittance amplitude as a function of layer thickness, ε_z ~ 6μm which leads to a cavity modal volume of ~ 0.6 λ^3. This is, to the best of our knowledge, the smallest 3D defect cavity ever made in the infrared wavelength.

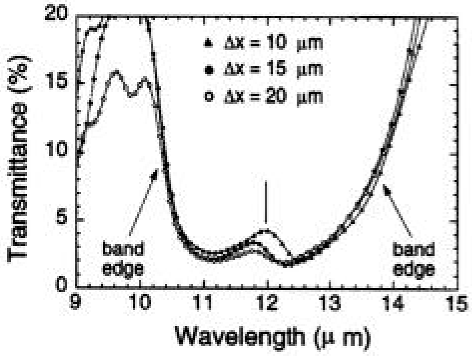

Fig.3

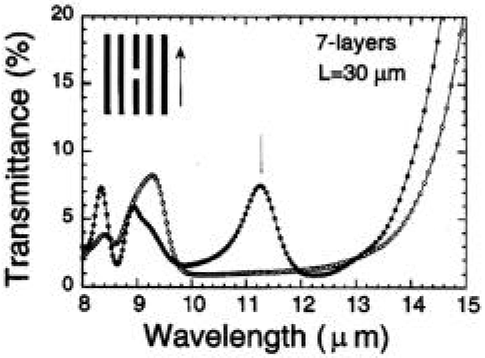

Fig.4

A theoretical model calculation suggests that the vacancy defect can only be excited by light polarized along the rod direction, i.e. the x-direction as indicated by the arrow in the inset of Fig.4. A schematic of the defect cavity and its wavefunction extend is also shown in the inset.Indeed, the data taken with x-polarization, solid dots, shows a single tranasmission peak centered at λ=11.2μm. The open dots are data taken with y-polarization and no transmission peak was observed in the gap regime, confirming the polarization dependent of a cavity mode.The peak transmission is 7%, or 11dB attenuation, and full-width-half maximun 0.8μm, or a cavity-Q of 14. The peak wavelength agrees well with our theoretical predition and the measured cavity-Q is also close to the predicted value of Q=13. With a 10-layer structure, a cavity-Q of 110 is expected

Summary

Basic 3D photonic crystal structures operating at optical wavelengths have all been experimentally realized in Si and GaAs. The next challenge in photonic crystal research is to integrate superior photonic-crystal devices on-chip compactly and effectively. The resulting optical sub-systems will have an enhanced optical functionality to meet, for example, the needs for high-bandwidth communication network. Another equally important challenge is in the integration of optically functional materials with a photonic crystal to achieve active photonic-crystal devices. Two distinct examples are the introduction of nonlinear materials for high speed optical switching and the infiltration of a gain medium for highly efficient light emitting applications.

Publication Lists

1. “2D and 3D Photonic Crystals Built with VLSI Tools", ***MRS Bulletin***, *Vol*. 26, p.627, August 2001.
2. “Micro-fabrication and nano-fabrication of photonic crystals”, p. 83***, Photonic Crystal and Light Localizations***, edited by C.M. Soukoulis, NATO ASI Series (2001).
3. “Quantitative analysis of bending efficiency in photonic crystal waveguide bends at 1.55 μm wavelengths”, ***Optics Letters, Vol. 26,*** p.286-288 (2001).
4. “A complete three-dimensional photonic band gap in a simple cubic structure”, ***J of Opt. Soc. Ame. B***, Vol. 18, 32 (2001).
5. “Three-dimensional control of light in a 2D photonic crystal slab”, ***Nature***, vol. 407, p.983-986 (2000).
6. “Experimental demonstration of highly efficient waveguiding in a 2D photonic crystal slab”, ***Optics Letters***, vol. 25, 1297 (2000).
7. “Enhancement and Suppression of thermal emission by a 3D photonic crystal”, ***Phys. Rev. B 62 (Rapid Communication), R2243*** (2000).
8. “A 3D optical photonic crystal”, ***IEEE Journal of Lightwave Technology***, Vol.17, p.1944 (1999).
9. “Waveguide bends in 3D layer by layer photonic band gap”, ***Microwave and Optics Tech. Letters,*** *23* p.56 (1999).
10. “ Photonic band gap micro-cavcities in three-dimensions”, ***Phys. Rev. B***59, R15, 579 (1999).
11. “A 3D photonic crystal with a stop band from 1.35 to 1.95 μm”, ***Optics Letters,*** *24*, p. 49 (1999).

Distribution

1	**MS9018**	**Central Technical Files, 8945-1**
2	**MS 0899**	**Technical Library, 9616**
1	**MS 0612**	**Review and Approval Desk, 9612, for DOE/OSTI**

1	**MS 0188**	**LDRD Office**
2	**MS 0603**	**Shawn Lin, 1743**
2	**MS 1080**	**J.G. Fleming, 1749**
2	**MS 1415**	**S.K. Lyo, 1123**
1	**MS 0603**	**Mial Warren, 1743**
1	**MS 0601**	**J. Simmons, 1123**
1	**MS 1080**	**H. Stewart, 1749**
1	**MS 1079**	**Dave Myers, 1700**